Intrinsic stickiness and chaos in open integrable billiards: Tiny border effects

M. S. Custódio and M. W. Beims*
Departamento de Física, Universidade Federal do Paraná, 81531-990 Curitiba, PR, Brazil
(Received 29 April 2010; revised manuscript received 20 October 2010; published 2 May 2011)

Rounding border effects at the escape point of open integrable billiards are analyzed via the escape-time statistics and emission angles. The model is the rectangular billiard and the shape of the escape point is assumed to have a semicircular form. Stickiness, chaos, and self-similar structures for the escape times and emission angles are generated inside "backgammon" like stripes of initial conditions. These stripes are born at the boundary between two different emission angles but with the same escape times and when rounding effects increase they start to overlap generating a very rich dynamics. Tiny rounded borders (around 0.1% from the whole billiard size) are shown to be sufficient to generate the sticky motion with power-law decay $\gamma_{\rm esc} = 1.27$, while borders larger than 10% are enough to produce escape times related to the chaotic motion. Escape exponents in the interval $1 < \gamma_{\rm esc} < 2$ are generated due to marginal unstable periodic orbits trapping alternately (in time) regular and chaotic trajectories.

DOI: 10.1103/PhysRevE.83.056201 PACS number(s): 05.45.Ac

I. INTRODUCTION

Experiments usually measure a signal (light, atoms, particles, current, etc.) which comes out from the system of interest. If the open channel (the escape point or hole) of the physical device, where the signal comes out, has a relevant size and shape, the signal may include information from inside the physical device *and* from the open channel itself. The shape and size of the open channel depends on experimental interests but also on how the device is built. For the dynamics in mesoscopic systems and nanostructures, for example, the shape and the size of the small open channel can present irregularities or defects which may induce undesirable changes in the out-coming signal. Such sometimes intrinsic irregularities affect the dynamics of particles which collide with them.

From the theoretical point of view it is very difficult to describe, in general, the dynamics of colliding particles with irregular boundaries. Therefore in recent years more and more attention has been given to the description of particles confined inside boundaries (or billiards) which present some *specific* edges, softness, etc. To mention some examples we have the edge roughness in quantum dots [1], unusual boundary conditions in two-dimensional billiards [2,3], soft billiards [4–6], effects of soft walls [7] and edge collisions [8] of interacting particles in a 1D billiard, rounding edge [9,10] and edge corrections [11] in a resonator, deformation of dielectric cavities [12], and edge diffractions and the corresponding semiclassical quantization [13,14], among others.

Differently from the above works, which focus on the boundaries of systems, here we analyze the effect of irregularities from the open channel itself. What is the effect of (rounded) open channels on the out-coming signal? To mention some examples, rounded open channels are common in experiments with semiconductor devices [15,16] and quantum cavities [17], where the open channels have a shape very similar to those shown in Fig. 1, which is the model used here (types I and II). In the above-mentioned experiments the dimension of the open channel (not its width, but the radius of the rounded border) related to the whole device is around 0.1% for type II borders (the smallest case) and around 30% for type I borders (the largest case). Since experiments measure a signal which comes out from the system of interest, how is it affected by such rounded borders? Is it possible that tiny rounded borders transform an integrable dynamics into a chaotic one? What is their influence on the dynamics in open nanodevices, conduction fluctuations in semiconductors [15,18], particle transport in nanostructures, cold atoms in open optical billiards [19], etc.? Recent works in this direction have analyzed the effect of the *width* [20–23] and the *location* [20,22,24,25] of the open channel on the escape rates of particles in open billiards. Besides that, from the theoretical point of view the description of open billiards is very challenging [26].

Using the example of a billiard model we show here that the *shape* or *structure* of the open channel induces stickiness [27–29] and a self-similar and chaotic output signal, even if the dynamics inside the billiard is originally regular. We consider that the device borders (or extremities), which delimit the holes in realistic open systems, are not single points, but have their own shape. In this work results are shown for the escape-time statistics and the emission angles θ_f in the open rectangular billiard shown in Fig. 1. While self-similar structures are clearly visible in the escape times (ETs) and escape angles, the sticky motion is observed by the power-law decay of the ET statistic. Although it is possible to detect and quantify sticky motion via the distribution of finite-time Lyapunov exponents [7,8,30–33], for the purpose of the present work it is more adequate to use the ET statistics. The fractal behavior of the ET dynamics was also shown recently in Bose-Einstein condensates [34] and trapped ultracold atoms [35] and in a vase-shaped cavity [36] and generic chaotic cavities [37], just to mention some examples.

The paper is organized as follows. Section II presents the model, defines the ETs used to detect the sticky behavior, and shows related numerical results. Sections III and IV show the rich dynamics generated by the rounded border: long-lived states and self-similar structures for the ETs and emission angles. In Sec. V we present our final remarks.

*mbeims@fisica.ufpr.br

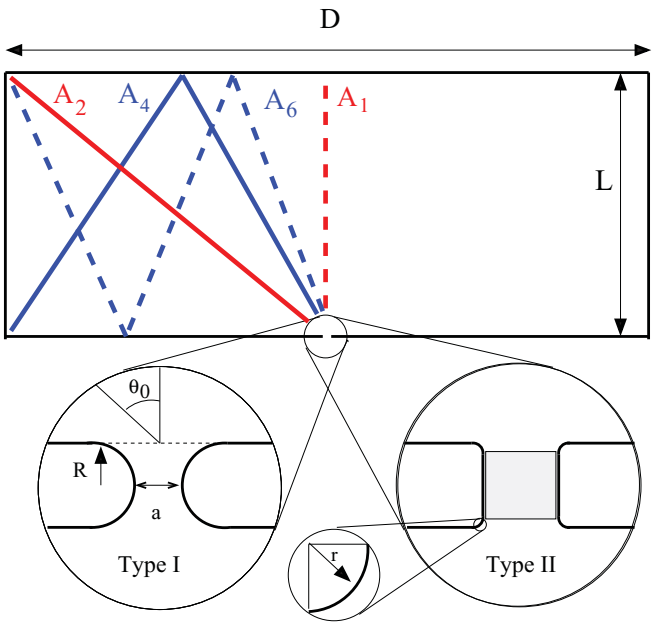

FIG. 1. (Color online) The rectangular billiard, with dimension $L \times D$, showing the open channels (borders) of type I (with radius R) and type II (radius $r \approx R/20$) considered here. The escape point lies exactly in the middle of the billiard. Initial angle θ_0 and, schematically, the shortest escape trajectories (A_1, A_2, A_4, and A_6) are shown. In all simulations we use $L = 4$ and $D = 10$.

II. ROUNDING BORDERS, POWER-LAW DECAYS, AND CHAOS

Stickiness is quantified through the recurrence-time statistics or the ET statistic, where the open channel is chosen as the recurrence region. Trajectories start at the open channel toward the inner part of the billiard. The time T is recorded when the trajectory returns to the open channel and leaves the billiard. The ET statistic is defined [38] by $Q(\tau) = \lim_{N\to\infty} \frac{N_\tau}{N}$, where N is the total number of recurrences and N_τ is the number of recurrences with time $T \geqslant \tau$. For systems with stickiness the ET statistic decays as a power law $Q(\tau) \propto \tau^{-\gamma_{\rm esc}}$ with $\gamma_{\rm esc} > 1$ being the scaling exponent. The precise definition of stickiness is related to the divergence of all higher moments of the mean recurrence time $\langle T \rangle$ (for details see [29,39,40]). We assume that there is stickiness when a power-law decay with $\gamma_{\rm esc} > 1$ is observed for two decades in time. Integrable billiards can have power-law decays with $\gamma_{\rm esc} = 1$ [41]. For hyperbolic chaotic systems and long times the ET statistic decays exponentially.

In the simulations particles start at times $t = 0$ from the open channel (uniformly distributed from $D/2 - a/2 \leqslant x_0 \leqslant D/2$) with an initial angle θ_0 toward the inner part of the billiard and with velocity $|\vec{v}| = 1$. The particle suffers elastic collisions at the billiard boundaries and at the rounded border of the open channel. For each initial condition we wait until the particle leaves the billiard and record θ_f and the escape time T. We use 10^5 initial conditions distributed uniformly in the interval $1.00 \times 10^{-6} \lesssim \theta_0 \lesssim 1.57$. The dynamics for $-\pi/2 \leqslant \theta_0 \leqslant 0.0$ is symmetric.

Without rounding effects ($R = r = 0.0$) the dynamics in the closed rectangular billiard is integrable, has zero Lyapunov exponents, and can be described in terms of invariant tori. This regular dynamics is shown in the phase space, Fig. 2(a), where the collision angle θ is plotted as a function of horizontal coordinate x. Straight lines parallel to the x axis are related to tori with irrational winding numbers. Periodic orbits are related to tori with rational winding numbers and are the marginally unstable periodic orbits (MUPOs) from this problem. When opening up the billiard, trajectories which start exactly on a rational torus will never leave the billiard, expect for those initial conditions which match the opening channel. Trajectories which start on an irrational torus will certainly escape the billiard after some time. However, MUPOs can trap these trajectories generating the power-law decay with $\gamma_{\rm esc} = 1$. This is exactly what is observed for the decay of $Q(\tau)$ in Fig. 3 for $R/L = 0.0$.

When the rounded border increases ($R/L > 0.0$) a chaotic component is introduced by the dispersing boundary and no regular islands are observed. Figure 2(b) shows the phase-space dynamics when $R/L = 0.1$ using just one initial condition. Blue (dark gray) points occur when the trajectory collides with the rounded border and defines the scattering region (SR) or chaotic region which occurs inside the interval $D/2 - a/2 - R \leqslant x \leqslant D/2 + a/2 + R$ [see blue (dark gray) region in Fig. 8]. Green (light gray) points occur when the trajectory collides with the vertical and horizontal parallel

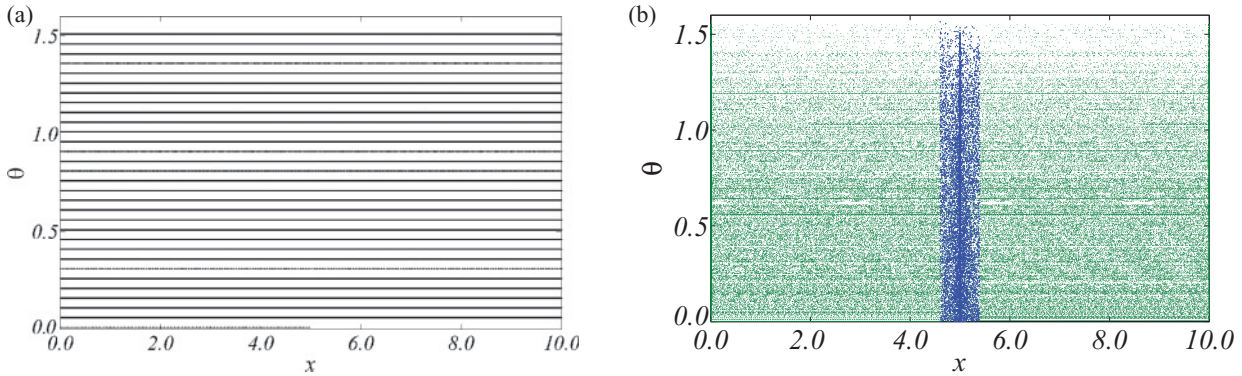

FIG. 2. (Color online) Phase-space dynamics for (a) $R = r = 0$ and (b) $R/L = 0.1$ (one initial condition). Blue (dark gray) points occur when the trajectory collides with the rounded border and defines the scattering region (SR) or chaotic region (see also Fig. 8). Green (light gray) points occur when the trajectory collides with the vertical and horizontal parallel walls.

walls, where the dynamics is regular and can be still described by irrational/rational tori. Thus outside the scattering region, where the trajectory does not collide with the rounded border, the dynamics is still regular. When the trajectory starts on a torus, it remains on it until it touches the rounded border of the opening channel. There it can be scattered to another torus, moving along this new torus until it touches again the rounded border, where it can be scattered again to another torus. This procedure repeats itself many times and the trajectory jumps between different tori so that for long enough times almost all irrational tori are visited. This can be seen by the many horizontal lines in the phase space of Fig. 2(b), which was obtained starting just on one torus with initial condition $\theta_0 = 0.85$. It is important to observe that the chaotic region occurs only inside the scattering region $4.5 \leqslant x \leqslant 5.5$ and acts like a chaotic layer which connects different irrational tori. MUPOs exist inside this region, such as all periodic orbits which collide with the bottom plane of the billiard but not with the rounded border, or the bouncing ball orbit colliding between the parallel vertical walls. Therefore, inside the scattering region chaotic trajectories are trapped by the MUPOs for the short times the MUPOs cross the scattering region. Outside this region we have only regular trajectories trapped by the MUPOs. It has been observed [23,38,42,43] that when MUPOs are immersed in a chaotic sea with sharply divided phase spaces, they generate sticky motion with a power-law decay with exponent $\gamma_{\rm esc} = 2$. Such decay, however, changes drastically when hierarchical phase spaces are present [42]. In our case we do not have a hierarchical phase space and the MUPOs are inside the chaotic sea only for small times. In fact, a sharply divided phase space occurs *in time* and trajectories are trapped inside the chaotic region, as can be seen by the higher density of points close to the center of the scattering region in Fig. 2(b). This higher density is the consequence of trajectories bouncing successively between the left and right rounded borders. As R/L increases more and more, the chaotic scattering region increases and an almost chaotic phase space is expected. It is worth mentioning that in dissipative systems it has been observed [44–47] that the trajectory switches between long times on the periodic attractor [negative finite-time Lyapunov exponents (FTLEs)] and smaller times on the chaotic saddle with positive FTLEs.

We start by discussing numerically the quantity $Q(\tau)$ for the type I billiard and for different values of the ratio R/L, where L is kept fixed. The results are shown in Fig. 3 for $a = 0.15$ and $R/L = 0.0, 1.0\times10^{-4}, 1.0\times10^{-3}, 1.0\times10^{-2}, 5.0\times10^{-2}, 1.0\times10^{-1}, 1.5\times10^{-1}, 3.0\times10^{-1}$, and 1.0. Note that these results are automatically applied to the type II billiard. The only difference is that for the type II billiard the escape time τ' is related to τ by $\tau + t_p$, where t_p is the time the trajectory needs to travel the two parallel boundaries from the escape hole (see type II border in Fig. 1). For comparison we show in Fig. 3 the straight lines with power-law decay exponents $\gamma_{\rm esc} = 1$ (dashed) and 2 (points). The first observation is that for $R/L = 0.0$ (curve i), $Q(\tau)$ has a power-law decay with $\gamma_{\rm esc} \sim 1$. The power law for this case is generated by all trajectories on irrational tori trapped by the periodic orbits from the rectangular billiard. This was checked by looking at the escape times as a function of the collision angles θ of the trajectories. All angles between $[-\pi/2, \pi/2]$

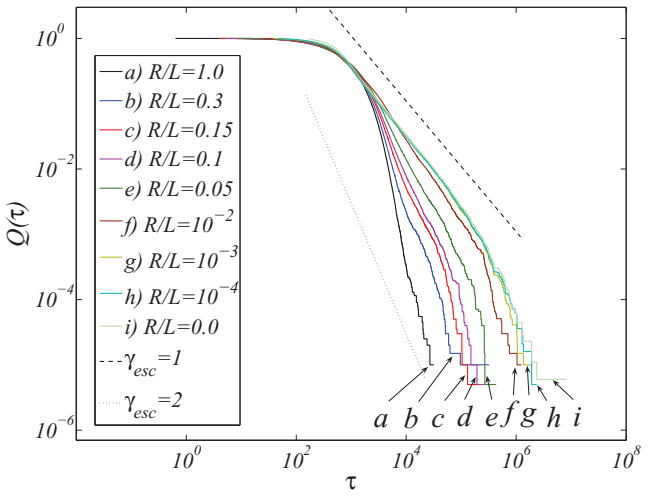

FIG. 3. (Color online) Behavior of $Q(\tau)$ for $a = 0.15$ and for different values of the ratio R/L (curves $a \to i$).

are relevant to generate longer escape times. Thus trajectories close to the periodic orbits inside the rectangle generate the power-law decay with $\gamma_{\rm esc} = 1$.

For very small rounding effects, $R/L = 10^{-4} \to 10^{-3}$ (curves $h \to g$), the qualitative behavior of $Q(\tau)$ approaches the $\gamma_{\rm esc} = 1$ decay obtained for the integrable case. This is expected since, as observed in the phase-space dynamics of Fig. 2(b), the chaotic scattering region is still very small and the MUPOs are most of the time surrounded by regular trajectories. Regular trajectories close to MUPOs generate the $\gamma_{\rm esc} = 1$ decay. This decay starts to change slowly for $R/L = 1.0\times10^{-2}$ (curve f), generating a decay with $1 < \gamma_{\rm esc} < 2$. In other words, we observe the effect of MUPOs trapping alternately (in time) regular and chaotic trajectories, making the exponent slowly change, $\gamma_{\rm esc} = 1 \to 2$ (see below). Since the scattering region increases with R/L, the MUPOs start to trap preferentially the chaotic trajectories, so that for $R/L = 1\times10^{-1}$ (curve d) the power-law decay approaches $\gamma_{\rm esc} \sim 2$. However, this decay occurs for just one and a half decades and cannot rigorously be characterized as stickiness. We guess that for smaller values of the aperture a, trajectories will stay longer inside the billiard and maybe the desired two decades can be observed. This will be discussed below. As R/L increases more and more ($\to 1.0$), the scattering region increase very much and an exponential decay is observed, typical of chaotic systems.

Figure 4 shows the $Q(\tau)$ dependence on the aperture a when $R/L = 0.01$ is kept fixed. Starting from below [$a = 0.4 \to 0.1$ (curves $j \to n$)], we observe two power-law decays: for shorter times, inside the dashed lines, $\gamma_{\rm esc} \sim 1$, and for intermediate and larger times, $\gamma_{\rm esc} \sim 1.27$. When a decreases, the first decay disappears giving place to the second decay. For $a = 0.08$ and 0.04 (curves $o \to p$) we have just one power-law decay with $\gamma_{\rm esc} \sim 1.27$ and it occurs for two decades. Thus the stickiness effect occurs for these values of a and R/L. The exponent $\gamma_{\rm esc} \sim 1.27$ arises from the following: In Fig. 2(b) we observed that the trajectory alternates in time between the chaotic (blue, dark gray) and regular motion (green, light gray). When the trajectory is close to MUPOs inside the chaotic region, the escape exponent tends to $\gamma_{\rm esc} \to 2$, but when it is

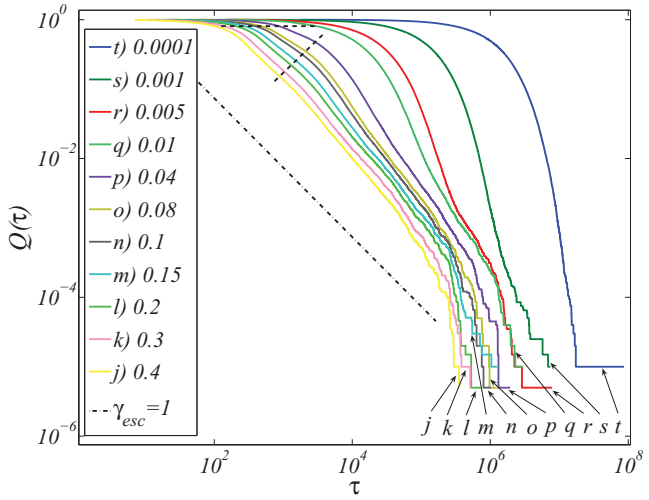

FIG. 4. (Color online) Behavior of $Q(\tau)$ for $R/L = 0.01$ and for different values of the aperture a.

close to MUPOs inside the regular region, the escape exponent tends to $\gamma_{\rm esc} \to 1$. Thus the overall exponent will be something in between ($\sim$1.27). It is also interesting to observe that decreasing a from 0.01 to 0.0001 (curves $q \to t$), the power-law decay is not observed for long times but is slowly substituted, from below (smaller times), by the exponential decay, typical of chaotic systems. This can be understood from the analysis of the phase-space dynamics: The chaotic scattering region is also the trapping region; thus as a decreases the time spent inside the billiard increases and therefore the amount of chaotic motion increases relative to the time MUPOs are inside the scattering region. Thus the exponential decay is preferred instead of the power-law decay with $\gamma_{\rm esc} = 2$. This also explains why we are not able to observe power-law decays for much longer times by just decreasing a. It changes the dynamics.

III. ROUNDING BORDERS GENERATING THE RICH DYNAMICS

The physics involved in the dynamics becomes more evident when the ETs and escape angles θ_f are plotted as function of the initial incoming angle θ_0 and for different ratios R/L. These plots are shown in Fig. 5 and were generated by using 500×500 points in the intervals $0.01 \leqslant \theta_0 \leqslant 1.57$ and $0.0001 \leqslant R/L \leqslant 1.0$ $[-9.2 \leqslant \ln(R/L) \leqslant 0.0]$. We start by discussing Fig. 5(a), where each color represents a given value of the ETs written as $\log(\tau)$ (see the color bar on the right: dark blue $\to$ yellow $\to$ white in the color scale and dark gray to white in the gray scale). Horizontal stripes with different colors are evident for a significant range of R/L values. Each stripe is defined by a bunch of initial conditions which lead to the same ET and consequently have the same color. For example, for some specific initial angles ($\theta_0 \sim 0.39, 0.56, 0.69, 0.89$) we observe dark blue (gray) stripes which correspond to very short ETs. For $R/L = 0$ these angles can be obtained analytically for periodic orbits (from the close billiard) with period $q = 2^n$. They are $\theta_0^{(n)} = \arctan[\frac{D}{2nL}]$ ($n = 1,2,3,\ldots$), which is the middle value of the main dark blue (gray) stripes which are born at $R/L = 0$. The corresponding ETs are $t_n = nt$, where t is ETs from the case $n = 1$, explained below. The shortest ET ($t_0 \sim 8.0$) occurs for $\theta_0 \sim 0.0$, where the particle collides once against the wall in front of the escape hole and then leaves the billiard (see trajectory A_1 in Fig. 1). The widths of the stripes are always related to the aperture a from the hole. The next shortest ET ($t_1 = t \sim 12.8$) occurs for $n = 1$ at $\theta^{(1)} = \arctan 5.0/4.0 \sim 0.89$, where the particle collides directly with the corner of the billiard (see trajectory A_2 in Fig. 1). The third shortest ET ($\sim 2t$) occurs for $\theta^{(2)} = \arctan 5.0/8.0 \sim 0.56$ and is shown by trajectory A_4 in Fig. 1. In the limit $\theta_0 \to \pi/2$ the ETs tend to increase since the trajectories are parallel to the escape point. As n increases the ETs from the trajectories A_{2n} increase, the corresponding stripes assume other colors [light blue (gray) $\to$ green (light gray) $\to$ yellow (white), see Fig. 5(a)] and their widths decrease. This is the main behavior of the ETs and stripes close to $R/L \sim 0.0$.

Increasing R/L we observe in Fig. 5(a) that the stripes from shorter ETs [dark blue (gray)] tend to survive longer the rounding border effect, while stripes with larger ETs [light blue (gray), green (light gray), and yellow (white)] tend to be destroyed, or even to mix themselves. As a matter of notation, we call the dark blue (gray) stripes the *main stripes* and the other stripes the *secondary stripes*. Therefore, secondary stripes are always related to intermediate and larger values of ETs. Outside the main stripes the dynamics becomes very rich and complex. It is important to mention that for $\theta_0 \to \pi/2$

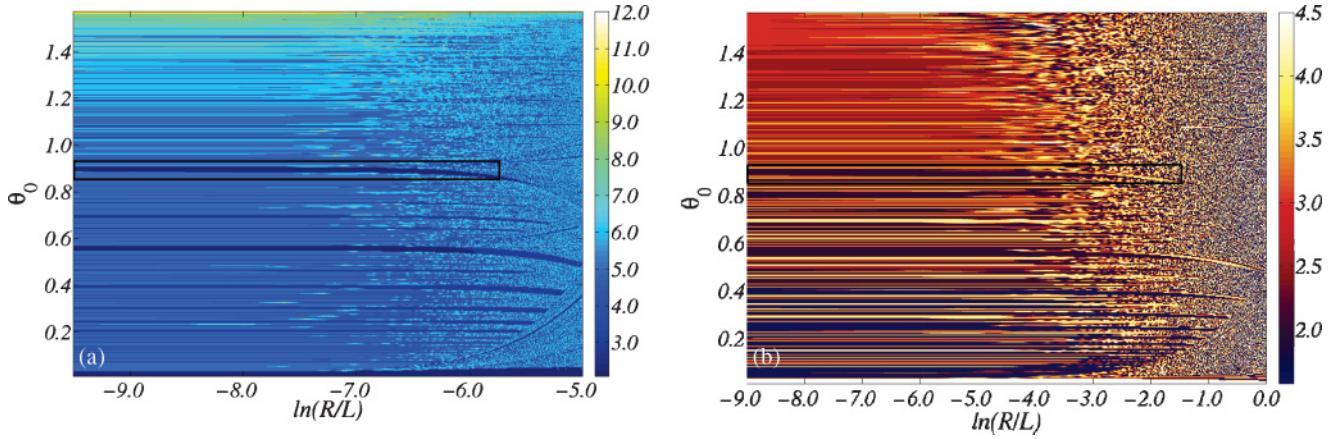

FIG. 5. (Color online) (a) Ln of the escape time and (b) emission angle θ_f as a function of $\ln(R/L)$ and θ_0.

(close to the horizontal MUPO) we observe that as $R/L \to 1$ the ETs decrease. This makes sense because trajectories close to the horizontal MUPOs are more easily scattered away when R/L increases. This is also the reason why the ETs in $Q(\tau)$ decrease when R/L increases, as observed in Fig. 3. Thus we have two opposite behaviors for the ETs when R/L increases: The ETs decrease when $\theta_0 \sim \pi/2$ but they increase inside secondary stripes. Before we explain how this second effect occurs we would like to bring to attention the rich dynamics generated by the rounding effects.

Figure 5(b) shows θ_f as a function of $\ln(R/L)$ and θ_0. Each color is now related to one emission angle θ_f (see the color bar on the right: dark blue $\to$ red $\to$ yellow $\to$ white in the color scale and dark gray to white in the gray scale). These emission angles vary between $\theta_f \sim 1.4$ (almost horizontally to the left) and $\theta_f \sim 4.5$ (almost horizontally to the right). As in Fig. 5(a), also here stripes with different colors are evident for a significant range of R/L values. Each stripe is defined by a bunch of initial conditions which lead to the same θ_f. In most cases these stripes occur for the same values of θ_0 from Fig. 5(a). However, two stripes with the same color (same ETs) in Fig. 5(a) do not necessarily have the same color (same θ_f) in Fig. 5(b). In other words, different escape angles can have the same ETs. As R/L increases more and more, some stripes survive while others are destroyed or mixed, as in Fig. 5(a). The emission angles show a very rich dynamics due to the increasing rounded borders, alternating between all possible colors.

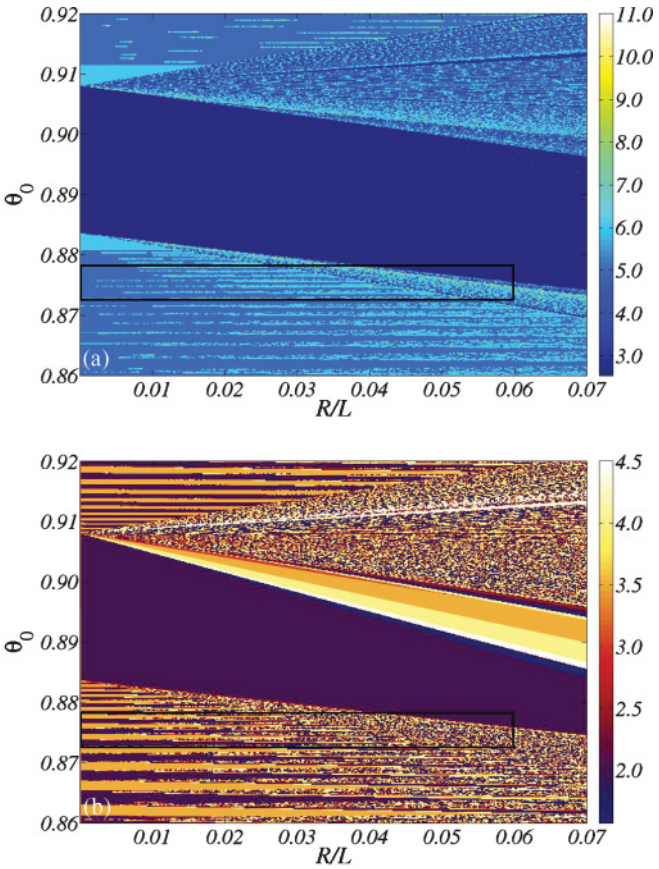

FIG. 6. (Color online) Magnifications from the boxes shown in Figs. 5(a) and 5(b).

IV. ROUNDING BORDERS GENERATING BACKGAMMON STRIPES

In Figs. 6(a) and 6(b) we show, respectively, a magnification for $\log(\tau)$ and θ_f. The magnification is taken around the trajectory A_2 (see Fig. 1) which has a short ET (main stripe). We observe in Fig. 6(a) that above the main stripe the ET dynamics changes significantly when R/L increases: Larger [light blue (gray) and yellow (white)] and shorter [dark blue (gray)] ETs appear inside a secondary stripe. The width of this secondary stripe increases linearly with R/L. For the emission angle [see Fig. 6(b)] we see a very rich dynamics emerging inside such a secondary stripe, alternating between all possible colors (all emission angles). In addition, below the main stripe a sequence of secondary stripes appear in the light blue (gray) background, as can observed in the magnification shown in Fig. 7(a). The width of each stripe in this sequence increases with R/L, resembling stripes from a backgammon board. As a matter of notation, secondary stripes with increasing width will be referred as "backgammon stripes." Stickiness and the power-law behavior with $\gamma_{\rm esc} > 1$ observed in Figs. 3 and 4 are born from initial angles which start inside the backgammon stripes. These are the initial conditions which collide, at least once, with the rounded border. For a given value of R/L they define the instability regions for the injection angles. The emergence of the power-law behavior becomes more evident if we compare Fig. 7(a) with the emission-angle behavior shown in Fig. 7(b). The light blue (gray) background observed in Fig. 7(a), which corresponds to *one* ET, has two colors [purple (black) and orange (white)] in Fig. 7(b), which correspond to *two* emission angles ($\sim$2.1 and $\sim$3.5). It is interesting that the sequence of backgammon stripes in Fig. 7(a), and the corresponding multicolor backgammon stripes from Fig. 7(b), are born exactly at the boundary between the purple (black) and orange (white) escape angles at $R/L \sim 0$. Inside the backgammon stripes the range of allowed ETs increases, as can be observed by the increasing number of light blue (gray) and yellow (white) points. The dynamics involved in the emission angles inside the backgammon stripes is also impressive, showing that tiny changes or errors in the initial angle may drastically change the emission angle. Observe that the dynamics *inside* the backgammon stripes is a consequence of trajectories which collide with the *inner part* of the semicircle from the escape channel, generating the power law with a tendency to change, $\gamma_{\rm esc} = 1 \to 2$ (see Figs. 3 and 4). This is important since such stripes allow us to characterize the different domains of the dynamics, from stable to unstable and from short to long ejection times. Another observation is that the location of the backgammon stripes itself is not self-similar, but *inside* the backgammon stripes the self-similar structure is evident. Many simulations (not shown) were performed to check this statement. A simple way to understand how the self-similar structure appears is shown in the example of Fig. 8. Two real trajectories starting, at the right rounded border, very close to each other, $\theta_0 = 0.895$ (green continuous line) and $\theta_0 = 0.897$ (red dot dashed line), collide once with the upper left corner of the billiard and return back to collide with the right rounded border. After that the green continuous line trajectory collides with the left rounded border

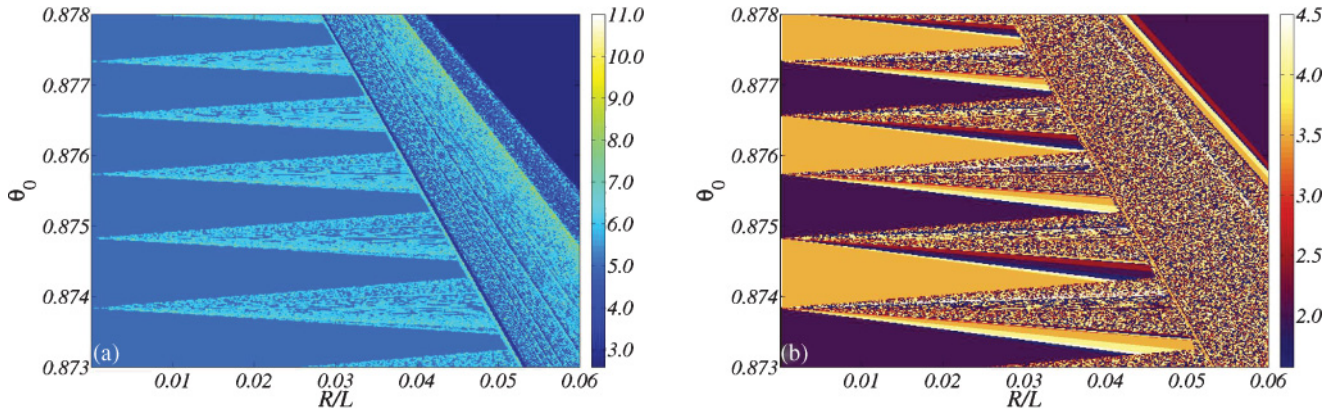

FIG. 7. (Color online) Magnifications from the boxes shown in Fig. 6.

and is scattered with an angle $\theta_s = 0.182$ in the direction of the upper horizontal wall. The red dot-dashed trajectory, however, passes tangentially to the left rounder border in the direction of the vertical wall, with an angle $\theta_s = 1.30$. Thus any initial angle between 0.895 and 0.897 will have a large number of trajectories with scattering angles between $\theta_s = 0.182$ and 1.30. This is just one example which occurs for trajectories which collide, at least twice, with the rounded border. For each collision with the rounded border this process can repeat itself. This shows the origin of the self-similar behavior for trajectories which collide with the rounded border. As R/L increases more and more, the self-similar regions increase very fast, *always* in the form of backgammon stripes which emerge at different initial angles at $R/L \sim 0.0$.

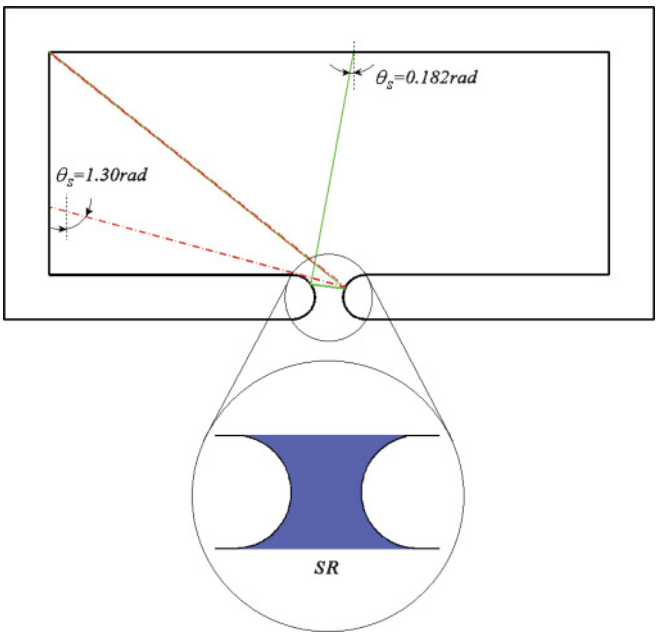

FIG. 8. (Color online) Two real trajectories starting, at the right rounded border, very close to each other $\theta_0 = 0.895$ (green continuous line) and $\theta_0 = 0.897$ (red dot dashed). After a few collisions, the scattering angle is respectively $\theta_s = 0.18$ and $\theta_s = 1.30$. The magnification shows the blue (gray) scattering region (SR).

The boundary of the stripes can be obtained analytically. Using simple geometrical relations, we obtain for the red (light gray) trajectory in Fig. 9 the condition

$$\tan\theta_+ = \frac{\varepsilon + R\sin(\alpha_+ - \theta_+)}{L + R - R\cos(\alpha_+ - \theta_+)}. \tag{1}$$

The solution of this equation gives the angle of a trajectory which collides, at least once, with the rounded border. The above relation can be used to obtain exact solutions for θ_+. We are interested in the limiting angle θ_+^*, between touching the rounded border and not. Thus we assume $\alpha_+ \sim \pi/2$ and the above equation gives

$$\theta_\pm^*(\varepsilon, L, R) \sim \arctan\left\{\frac{R(L+R) \pm \varepsilon\sqrt{L^2 + 2LR + \varepsilon^2}}{-\varepsilon R \pm (L+R)\sqrt{L^2 + 2LR + \varepsilon^2}}\right\}. \tag{2}$$

Two solutions are obtained: one for the red (light gray) trajectory in Fig. 9 with $\theta_+^*(\varepsilon, L, R)$ and one for the blue (gray) trajectory with $\theta_-^*(\varepsilon, L, R)$. For angles in the interval $\theta_-^*(\varepsilon, L, R) < \theta < \theta_+^*(\varepsilon, L, R)$ trajectories collide, at least once, with the rounded border. We start by discussing results for the case $\varepsilon \neq 0$. If we use $\varepsilon = D/2 = 5.0$, for example, we will look at the effect of the rounded border on the trajectory A_2 from Fig. 1, which has an initial angle $\theta_0 \sim 0.89$. The limiting angles $\theta_\pm^*(\varepsilon = 5, L = 4, R)$ are plotted in Fig. 10(a) showing that they increase unsymmetrically around the initial

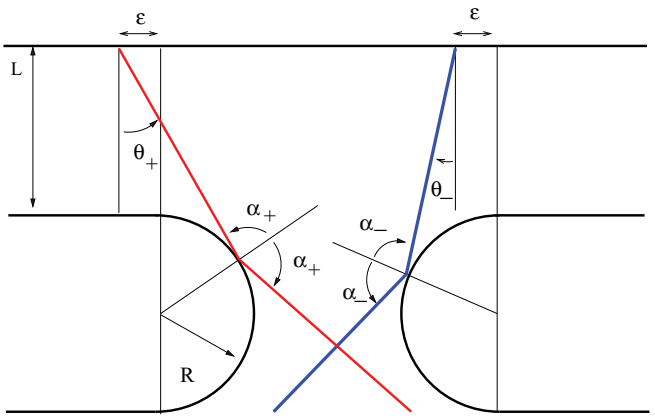

FIG. 9. (Color online) Schematic trajectories before escaping.

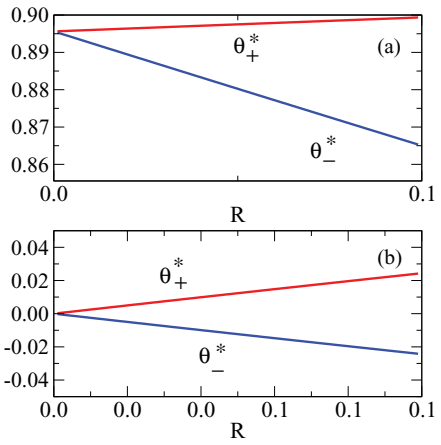

FIG. 10. (Color online) Limiting angles θ_+^* and θ_-^* as a function of R, determining the boundary of the secondary stripes.

angle. All angles inside these curves collide, at least once, with the rounded border. If we do not take into account the width of primarily stripes, the behavior of θ_+^* and θ_-^* follows exactly the secondary stripes observed in the numerical simulations from Fig. 6(b) around $\theta_0 \sim 0.91$ (the difference in the angles is due to the width of stripes in the numerical simulations for $R/L = 0$). Similar curves can be obtained for other values of ε; each one is related to a given trajectory. For $\varepsilon = 0$ Fig. 10(b) shows the behavior of $\theta_\pm^*(\varepsilon = 0, L = 4, R)$ as a function of R. It shows exactly the form of the backgammon stripes, which increase symmetrically around $\theta_0 = 0$. It is also possible to obtain such symmetrical curves for the backgammon stripes around angles $\theta_0 \neq 0$ by plotting $\theta_+^*(\varepsilon, L, R)$ and $\theta_-^*(-\varepsilon, L, R)$ for $\varepsilon \neq 0$. Therefore, all boundaries of the secondary stripes can be obtained from the angles $\theta_\pm^*(\pm\varepsilon, L, R)$. In addition, all trajectories with angles inside the interval $\theta_-^*(\varepsilon, L, R) < \theta < \theta_+^*(\varepsilon, L, R)$, which do not escape the billiard after one collision, will be scattered back, repeating the whole process, allowing now second, third, etc., collisions with the rounded border. Thus, any small initial angle in the interval between $\theta_-^*(\varepsilon, L, R)$ and $\theta_+^*(\varepsilon, L, R)$ may allow a large number of ejection angles and the self-similar structure becomes evident again.

V. CONCLUSIONS

Since experiments usually measure a signal coming out from the system of interest, the description of open physical devices is of utmost relevance. For experiments at the frontier of technological limitations, the open channel (the escape point or hole) can present irregularities or defects which may induce undesirable and intrinsic changes in the out-coming signal.

In this work we show that rounded borders in the open channel generate a rich dynamics in the integrable rectangular billiard. The escape-time statistics in the integrable billiard obeys a power-law decay with exponent $\gamma_{\rm esc} = 1$. When rounded borders of around $0.1\% \to 10\%$ from the whole billiard size are introduced, the exponent $\gamma_{\rm esc}$ tends slowly to change from $1 \to 2$. Such exponents arise due to the following dynamics in phase space: When trajectories are close to MUPOs immersed inside the chaotic region (our scattering region), the escape exponent $\gamma_{\rm esc}$ tends to the value 2, but when they are close to MUPOs immersed in the regular region, the escape exponent tends to 1. Since trajectories continuously switch between chaotic and regular regions, without selecting preferentially one of them, the overall escape exponent converges to something between 1 and 2. The cases in which we observe power-law decays for two decades, and thus stickiness, occur by keeping $R/L = 0.01$ fixed and changing the open channel aperture in the interval $a = 0.08 \to 0.04$. The related exponent is $\gamma_{\rm esc} \sim 1.27$. All exponents are independent of the *location* of the open channel along the horizontal wall. According to recent works [25], decay exponents change for holes located at distinct points when the smallest period of periodic orbits inside the different holes changes. In our case, for any location of the open channel along the horizontal axis, the smallest period is always equal to 1, which is related to the vertical periodic orbit A_1 shown in Fig. 1. Thus our power-law decay exponents are independent of the location of the open channel along the horizontal wall. It is interesting to observe that by decreasing a from 0.01 to 0.0001 the power-law decay is slowly substituted by the exponential decay, typical of chaotic systems. This can be explained since the chaotic scattering region is also the trapping region. Thus as a decreases, the time spent inside the billiard increases, and consequently the time inside the trapping region. Therefore, the amount of chaotic motion relative to the time MUPOs travel inside the chaotic region increases, and the exponential decay is preferred instead the power-law decay. In other words, for such small values of a and R/L, the time MUPOs travel inside the chaotic region is too small to trap the chaotic trajectories in order to generate the power law with $\gamma_{\rm esc}$. This is also the reason why we were not able to observe, besides the stickiness cases mentioned above, power-law decays longer than two decades by just decreasing a. For larger rounded borders ($>10\%$) the scattering region increases and the chaotic component becomes larger, so that an exponential decay is observed for the escape times, typical of chaotic motion.

Emission angles and escape times show a self-similar structure only for initial angles inside backgammon like stripes which are born at the integrable case $R/L = 0$. As R/L increases, the backgammon stripes increase more and more as was observed numerically and by the analytical solution (2). Trajectories which start inside the backgammon stripes will collide, at least once, with the rounded border, generating the rich dynamics, power-law decays, and chaotic motion. These stripes allow us to characterize the different domains of the dynamics, from stable to unstable and from short to long ejection times.

From the nonlinear perspective our results are impressive, showing that a very rich dynamics and stickiness may come alone from tiny border effects ($\sim 0.1\% \to 10\%$) in integrable billiards. Such effects should be visible directly in experiments with open integrable devices, open systems with leaks (see [20] and therein cited references), and in problems related to conduction fluctuations in semiconductors [15,18], particle transport in nanostructures, and cold atoms in open optical billiards [19].

Instead of rounded borders, other shapes for the open channels could be used. All of them (except for some trivial geometry) should generate a power-law decay and chaotic motion in integrable billiards, strongly affecting the out-coming signal. In this work we considered an integrable billiard as the starting point. We also performed extensive

numerical simulations to study rounded border effects in the stadium billiard, which is already chaotic without border effects ($R/L = 0$). For all values of R/L we found that the escape-time statistic has an exponential decay, expected for the chaotic behavior. For systems with mixed phase space we anticipate strong variation in the escape-time decay [42].

ACKNOWLEDGMENTS

The authors thank CNPq, CAPES, and FINEP (under project CT-INFRA/UFPR) for partial financial support. They also thank E. Altmann and C. Manchein for helpful discussions, and the anonymous referees for useful suggestions.

[1] F. Libisch, C. Stampfer, and J. Burgdörfer, Phys. Rev. B **79**, 115423 (2009).
[2] E. Bogomolny, M. R. Dennis, and D. Dubertrand, J. Phys. A **41**, 335102 (2009).
[3] M. V. Berry and M. R. Dennis, J. Phys. A **41**, 135203 (2008).
[4] P. Baldwin, Physica D **29**, 321 (1988).
[5] A. Knauf, Physica D **36**, 259 (1989).
[6] D. Turaev and V. Rom-Kedar, J. Stat. Phys. **112**, 765 (2003).
[7] H. A. Oliveira, C. Manchein, and M. W. Beims, Phys. Rev. E **78**, 046208 (2008).
[8] M. W. Beims, C. Manchein, and J. M. Rost, Phys. Rev. E **76**, 056203 (2007).
[9] M. S. Custódio and M. W. Beims, J. Phys. Conf. Ser. **246**, 012004 (2010).
[10] J. Wiersig, Phys. Rev. A **67**, 023807 (2003).
[11] C. Vaa, P. M. Koch, and R. Blümel, Phys. Rev. E **72**, 056211 (2005).
[12] R. Dubertrand, E. Bogomolny, N. Djellali, M. Lebental, and C. Schmit, Phys. Rev. A **77**, 013804 (2008).
[13] H. Bruus and N. D. Whelan, Nonlinearity **9**, 1023 (1996).
[14] D. Alonso and P. Gaspard, J. Phys. A **27**, 1599 (1994).
[15] C. Marlow *et al*., Phys. Rev. B **73**, 195318 (2006).
[16] A. S. Sachrajda, R. Ketzmerick, C. Gould, Y. Feng, P. J. Kelly, A. Delage, and Z. Wasilewski, Phys. Rev. Lett. **80**, 1948 (1998).
[17] Y. Takagaki, M. ElHassan, A. Shailos, C. Prasad, J. P. Bird, D. K. Ferry, K. H. Ploog, L.-H. Lin, N. Aoki, and Y. Ochiai, Phys. Rev. B **62**, 10255 (2000).
[18] H. Hennig, R. Fleischmann, L. Hufnagel, and T. Geisel, Phys. Rev. E **76**, 015202 (2007).
[19] A. Kaplan, N. Friedman, M. Andersen, and N. Davidson, Phys. Rev. Lett. **87**, 274101 (2001).
[20] E. G. Altmann and T. Tél, Phys. Rev. E **79**, 016204 (2009).
[21] C. P. Dettmann and O. Georgiou, Physica D **238**, 2395 (2009).
[22] L. A. Bunimovich and C. P. Dettmann, Europhys. Lett. **80**, 40001 (2007).
[23] D. N. Armstead, B. R. Hunt, and E. Ott, Physica D **193**, 96 (2004).
[24] M. Demers, P. Wright, and L. S. Young, Commun. Math. Phys. **294**, 353 (2010).
[25] L. Bunimovich and A. Yutchenko, Discrete and Continuous Dynamical Systems-Series B **9**, 37 (2008).
[26] C. P. Dettmann, e-print arXiv:1007.4166.
[27] C. F. F. Karney, Physica D **8**, 360 (1983).
[28] K. K. R. J. Bagley, Phys. Lett. A **110**, 435 (1985).
[29] G. M. Zaslavski, Phys. Rep. **371**, 461 (2002).
[30] S. Tomsovic and A. Lakshminarayan, Phys. Rev. E **76**, 036207 (2007).
[31] C. Manchein, M. W. Beims, and J. M. Rost, e-print arXiv:0907.4181.
[32] R. Artuso and C. Manchein, Phys. Rev. E **80**, 036210 (2009).
[33] C. Manchein and M. W. Beims, Chaos Solitons Fractals **39**, 2041 (2009).
[34] K. A. Mitchell and B. Ilan, Phys. Rev. A **80**, 043406 (2009).
[35] K. A. Mitchell and D. A. Steck, Phys. Rev. A **76**, 031403 (2007).
[36] P. Hansen, K. A. Mitchell, and J. B. Delos, Phys. Rev. E **73**, 066226 (2006).
[37] R. Ketzmerick, Phys. Rev. B **54**, 10841 (1996).
[38] E. G. Altmann, A. Motter, and H. Kantz, Chaos **15**, 033105 (2005).
[39] G. M. Zaslavsky, Physica D **168**, 292 (2002).
[40] E. G. Altmann, Ph.D. thesis, Max Planck Institute for the Physics of Complex Systems, 2007.
[41] W. Bauer and G. F. Bertsch, Phys. Rev. Lett. **65**, 2213 (1990).
[42] E. G. Altmann, A. E. Motter, and H. Kantz, Phys. Rev. E **73**, 026207 (2006).
[43] P. Gaspard and J. R. Dorfman, Phys. Rev. E **52**, 3525 (1995).
[44] X. Wang, M. Zahn, C. H. Lai, and Y. C. Lai, Phys. Rev. Lett. **92**, 074102 (2004).
[45] A. P. S. S. Negi and R. Ramaswami, Int. J. Bifurcation Chaos Appl. Sci. Eng. **11**, 291 (2001).
[46] U. Feudel, J. Kurths, and A. S. Pikovsky, Physica D **88**, 173 (1995).
[47] C. Grebogi, E. Ott, S. Pelikan, and J. A. Yorke, Physica D **13**, 261 (1984).